Theoretical analysis of the role of Coulomb interactions in single and double photoionization of the helium dimer using numerical model simulations

Hongcheng Ni and Andreas Becker
JILA and Department of Physics, University of Colorado, Boulder, Colorado 80309-0440, USA
(Received 30 December 2013; published 4 March 2014)

Based on the results of numerical simulations we study scattering effects in single and double photoionization of the helium dimer. To this end we use a planar two-active-electron model of the helium dimer and abridged Hamiltonians in which different interactions between the electrons and the laser field and/or between the charged particles are removed from the full Hamiltonian. By comparing photoelectron angular distributions obtained in respective numerical simulations we are able to identify the role of the Coulomb interactions between the electrons and between the electrons and the nuclei for the primary as well as the knock-off electron in the processes.

DOI: 10.1103/PhysRevA.89.033402 PACS number(s): 33.80.Eh, 34.80.Dp, 36.40.−c

I. INTRODUCTION

The Coulomb interaction between charged particles, i.e., electrons and nuclei, is the basis of the structure of matter and the correlated dynamics of these charged particles in processes like chemical reactions. Accomplishments in experiment and theory over the past decade have greatly advanced our understanding of dynamical few-body problems, such as charged particle impact ionization or photoionization of atoms and small molecules. The development of a variety of theoretical approaches (e.g., [1,2]) as well as novel measurement techniques, e.g., the cold-target recoil-ion momentum spectroscopy technique [3], have contributed much to this progress.

Double ionization of a target due to the absorption of light is one of the dynamical few-body processes, which is strongly influenced by the Coulomb interactions between three, four, or even more particles. The technological progress in the development of a variety of light sources (synchrotron radiation [4], ultrashort intense lasers [5,6], and free-electron lasers [7–9]) over the past decades has allowed us to gain insights into different aspects of the dynamics of the correlated emission of two electrons from an atom or molecule. For example, studies on double photoionization with synchrotron radiation have advanced our understanding of the long-range character of the interaction between three or four charged particles in the Coulomb continuum (e.g., [1,2,4]).

Ab initio calculations, in particular the full time-dependent numerical simulations of the corresponding Schrödinger equation, have become available for certain few-body problems in recent years. While these calculations often provide excellent agreement with experimental data, the role of the interaction between each pair of charged particles during the single and double photoionization processes is often difficult to analyze. In a numerical simulation, in principle, it is possible to remove interactions between certain pairs of particles in the Hamiltonian and compare the results to those obtained with the full Hamiltonian. However, using this technique in an atomic or typical molecular system, the initial state inevitably changes as compared to the full simulation. Consequently, it is difficult to distinguish between the influence of the initial state and dynamic effects when analyzing the role of the removed interactions. In this respect, rare gas dimers are interesting systems, since they are formed via the weakly attractive van der Waals interaction between two rare gas atoms at much larger equilibrium distances than those of typical diatomic molecules. Due to the large internuclear separation and almost negligible overlap between the orbitals of the two atoms, changes in the initial state are small when certain interactions are removed.

Recently, experiments and theoretical analysis have been performed to study the double photoionization process of the helium dimer [10,11]. Interpretation of the experimental observations and theoretical results show that a two-step process leads to the double photoionization of the dimer for low photon energies. A primary electron localized at one atom in the helium dimer absorbs the photon energy from the laser field, then propagates along the internuclear axis and transfers its energy to a second electron in the neighboring helium atom. This process is called knock-off in view of the close analogy to a similar mechanism known in the double photoionization of atoms [12]. As we will show in this paper, in this molecule it is possible to study the role of individual Coulomb interactions during the single and double photoionization in *ab initio* numerical simulations. To this end, we consider abridged Hamiltonians, in which certain Coulomb interactions are removed without noticeable change in the initial state. We then compare the angular distributions obtained using the abridged Hamiltonian to those obtained with the full Hamiltonian. In this way we are able to identify the role of each Coulomb interaction during the process. Moreover, we are also able to distinguish and compare the angular distributions of the primary electron and the knock-off electron by removing the coupling between one electron and the laser field from the full Hamiltonian.

The remainder of the article is organized as follows. In Sec. II we briefly outline the planar two-active-electron model of the helium dimer used in the simulations [11], and then introduce and discuss different abridged Hamiltonians in which certain interactions are removed from the full Hamiltonian. A comparison between the ground states of the full and the abridged Hamiltonians will be given and discussed. In Sec. III we apply the different Hamiltonians in numerical simulations to study scattering effects of the photoelectron in single photoionization. In Sec. IV we consider double photoionization of the dimer model. We first analyze the projection to different final states in the calculations, then

we proceed to compare angular distributions of the primary and knock-off electron as well as to study the role of Coulomb interactions in the process. We end with a summary of our results.

II. THEORY

In this section we outline the four-dimensional model Hamiltonian used for the helium dimer in the simulations. We then present options to restrict the full model Hamiltonian in numerical simulations in order to label the electrons and analyze the effect of certain interactions on the single and double photoionization processes.

A. Four-dimensional model Hamiltonian

As shown in Fig. 1, we use a planar two-active-electron model of the helium dimer, in which the electrons are located at different atoms in the dimer and their dynamics is constrained to the same plane. The dimer axis is chosen to be fixed in space, parallel to the XUV laser field, which is assumed to be linearly polarized in the z direction, unless explicitly stated otherwise. It is further assumed that the emission of the electron proceeds fast enough to keep the internuclear distance R between the atoms in the dimer fixed during the simulations. Thus, in our model the dynamics of each electron is restricted to two spatial dimensions, and the corresponding four-dimensional model Hamiltonian is given by (Hartree atomic units, $e = m_e = \hbar = 1$, are used throughout the paper) [11]

$$\begin{aligned} H = &\frac{p_{x_1}^2 + p_{z_1}^2}{2} + \frac{p_{x_2}^2 + p_{z_2}^2}{2} + E(t)\,(z_1 + z_2) \\ &+ V_{\mathrm{SAE}}(r_{11}) + V_{\mathrm{SAE}}(r_{12}) + V_{\mathrm{SAE}}(r_{21}) + V_{\mathrm{SAE}}(r_{22}) \\ &+ \frac{1}{\sqrt{(x_1 - x_2)^2 + (z_1 - z_2)^2 + b^2}} + \frac{1}{R}, \end{aligned} \tag{1}$$

where $\boldsymbol{p}_i = (p_{x_i}, p_{z_i})$ and $\boldsymbol{r}_i = (x_i, z_i)$ (with $i = 1,2$) are the momentum operators and spatial coordinates of the two active electrons. The linearly polarized laser field is given in the form of

$$E(t) = \cos^2\left(\frac{\omega t}{2N}\right)\cos\left(\omega t + \phi\right), \tag{2}$$

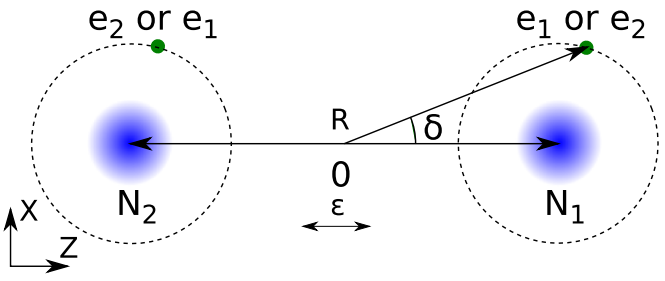

FIG. 1. (Color online) Scheme of the model for the helium dimer [11]. One electron at each atom is considered to be active and the electrons are restricted to the same plane. The internuclear distance R and the dimer axis are fixed in space. The dimer axis is chosen parallel to the laser polarization direction ε during the simulations, unless explicitly stated otherwise.

where ω is the central frequency, N is the number of cycles, and ϕ is the carrier-envelope phase of the laser pulse, which is set to $-\pi/2$ in the present simulations. The distance between ith electron and jth nucleus ($i, j = 1,2$) is given by

$$\begin{aligned} r_{ij} = \Bigg[&\left(x_i + \frac{(-1)^j R}{2}\sin\theta\right)^2 \\ &+ \left(z_i + \frac{(-1)^j R}{2}\cos\theta\right)^2 + a^2\Bigg]^{1/2}, \end{aligned} \tag{3}$$

where $a^2 = 0.201$ and $b^2 = 0.01$ denote soft-core parameters and $\theta = 0$ is the angle between the dimer axis and the laser polarization axis, representing parallel orientation, unless explicitly stated otherwise. We used a single active electron (SAE) potential for the helium atom [13]

$$V_{\mathrm{SAE}}(r) = -\frac{Z_c + a_1 e^{-a_2 r} + a_3 r e^{-a_4 r} + a_5 e^{-a_6 r}}{r}, \tag{4}$$

with $Z_c = 1.0$, $a_1 = 1.231$, $a_2 = 0.662$, $a_3 = -1.325$, $a_4 = 1.236$, $a_5 = -0.231$, and $a_6 = 0.480$.

B. Reduction of model Hamiltonian

For further analysis we used abridged Hamiltonians in test simulations, in which certain interaction terms are removed from the full model Hamiltonian [Eq. (1)]. One goal to use these reductions was to distinguish the primary electron, which first interacts with the light field, from the secondary electron by labeling the two electrons. This can be done by removing the term $E(t)z_2$ from the full Hamiltonian, which gives

$$\begin{aligned} H_{\mathrm{E1}} = &\frac{p_{x_1}^2 + p_{z_1}^2}{2} + \frac{p_{x_2}^2 + p_{z_2}^2}{2} + E(t) z_1 \\ &+ V_{\mathrm{SAE}}(r_{11}) + V_{\mathrm{SAE}}(r_{12}) + V_{\mathrm{SAE}}(r_{21}) + V_{\mathrm{SAE}}(r_{22}) \\ &+ \frac{1}{\sqrt{(x_1 - x_2)^2 + (z_1 - z_2)^2 + b^2}} + \frac{1}{R}. \end{aligned} \tag{5}$$

In the corresponding test simulations we can then identify electron 1 as the primary and electron 2 as the secondary or knock-off electron in double photoionization and, thus, compare the angular distributions for these electrons.

The present model of the helium dimer further facilitates the analysis of dynamical effects due to the interactions between electrons and nuclei. As mentioned above, the two electrons are initially predominantly located at different atoms in the dimer. This can also be seen from the spatial distributions of the lowest energy eigenstates of the planar helium dimer model, which are shown in Fig. 2 for an internuclear separation of $R = 5.6$ a.u. corresponding to the minimum of the helium dimer potential [14]. These energy eigenstates were obtained via imaginary time propagation. The initial guess state for the imaginary time propagation was chosen to be a 4D Gaussian wave function. The spatial distributions are shown as functions of z_1 and z_2 and are integrated over the other coordinates. The ground state [Fig. 2(a)] is a singlet state, while the first excited state [Fig. 2(b)] is a triplet state.

Due to the large internuclear distance, the interaction of each electron with the distant nucleus in the initial dimer state is rather small. Hence, in two further abridged Hamiltonians, we neglected first the interaction of electron 2 with nucleus 1,

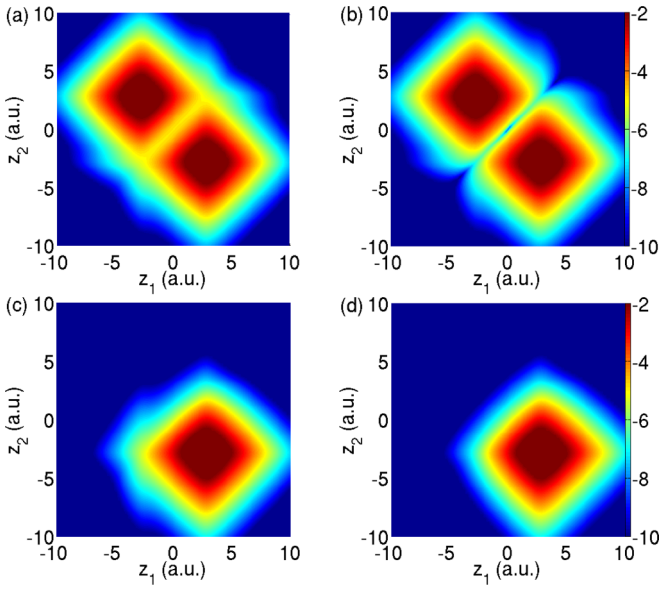

FIG. 2. (Color online) Spatial distributions (on a logarithmic scale) of the (a) ground state and (b) first excited state of the planar model helium dimer with full model Hamiltonian and that of the ground states of the planar model helium dimer with abridged Hamiltonians (c) $H_{\mathrm{E1,local1}}$ [Eq. (6)] and (d) $H_{\mathrm{E1,local2}}$ [Eq. (7)]. The distributions are integrated over x_1 and x_2 and shown as functions of z_1 and z_2.

$V_{\mathrm{SAE}}(r_{21})$, to get

$$H_{\mathrm{E1,local1}} = \frac{p_{x_1}^2 + p_{z_1}^2}{2} + \frac{p_{x_2}^2 + p_{z_2}^2}{2} + E(t)z_1 + V_{\mathrm{SAE}}(r_{11}) + V_{\mathrm{SAE}}(r_{12}) + V_{\mathrm{SAE}}(r_{22}) + \frac{1}{\sqrt{(x_1 - x_2)^2 + (z_1 - z_2)^2 + b^2}} + \frac{1}{R}, \quad (6)$$

and then $V_{\mathrm{SAE}}(r_{21})$ as well as $V_{\mathrm{SAE}}(r_{12})$ to get

$$H_{\mathrm{E1,local2}} = \frac{p_{x_1}^2 + p_{z_1}^2}{2} + \frac{p_{x_2}^2 + p_{z_2}^2}{2} + E(t)z_1 + V_{\mathrm{SAE}}(r_{11}) + V_{\mathrm{SAE}}(r_{22}) + \frac{1}{\sqrt{(x_1 - x_2)^2 + (z_1 - z_2)^2 + b^2}} + \frac{1}{R}. \quad (7)$$

In the first of the two Hamiltonians, $H_{\mathrm{E1,local1}}$, the symmetry of the electron-nucleus interactions is removed and, therefore, the electrons are localized at one of the two nuclei, i.e., electron 1 at nucleus 1 and electron 2 at nucleus 2, as can be seen from the ground state distribution shown in Fig. 2(c). We note that in this Hamiltonian all the interactions of the primary electron, i.e., electron 1, which interacts with the light field, are retained. On the other hand, in $H_{\mathrm{E1,local2}}$ the interaction of the primary electron with the second nucleus (nucleus 2) is removed as well and the corresponding initial state is represented in Fig. 2(d). As we will show below, comparison of the results from the simulations with the different Hamiltonians enables us to study, e.g., the scattering of the primary electron at the second nucleus (nucleus 2) in the photoelectron angular distributions.

We note that due to the localization of the electrons at either one of the nuclei, the corresponding ground states are no longer symmetric with respect to the exchange of electrons and the terminology of singlet and triplet states does not apply to the states of the two abridged Hamiltonians. The difference between the ground states of the full and the two abridged Hamiltonians can be quantified via their overlaps as

$$\left|\left\langle \psi_{\mathrm{E1,local1}} \middle| \psi_{\mathrm{full}}^{\mathrm{singlet}} \right\rangle\right|^2 = 0.499\,562, \quad (8)$$

$$\left|\left\langle \psi_{\mathrm{E1,local2}} \middle| \psi_{\mathrm{full}}^{\mathrm{singlet}} \right\rangle\right|^2 = 0.498\,898. \quad (9)$$

Both overlaps (as well as those with the triplet state of the full Hamiltonian) are close to 0.5, indicating the small effect of the interaction between an electron, localized at one atom in the dimer, and the distant nucleus in the initial state. The value of 0.5 instead of 1.0 arises due to the localization of each electron at one of the two nuclei in the abridged Hamiltonians.

C. Numerical simulations

The time-dependent Schrödinger equations (TDSE) corresponding to the full model Hamiltonian as well as the three abridged Hamiltonians are solved using the Crank-Nicolson method on a grid with $N_{x_1} = N_{x_2} = 200$ and $N_{z_1} = N_{z_2} = 300$ grid points, a grid step of $\Delta x_1 = \Delta x_2 = \Delta z_1 = \Delta z_2 = 0.3$, and a time step of $\Delta t = 0.05$. In the simulations the interaction with a four-cycle XUV laser pulse at a central wavelength of 20 nm and a peak intensity of 1×10^{14} W/cm^2 was used. We employed absorbing boundaries of the form $\cos^{1/6}(\frac{\pi}{2}\frac{|x-x_0|}{L})$ with $|x| \geqslant |x_0|$, where x_0 denotes the border of the boundary region and L its width. The boundary was chosen to span 10% of the grid size in each direction.

In order to analyze single and double photoionization of the helium dimer via the corresponding electron angular distributions, we stopped the simulations before the respective part of the wave function reached the boundaries. We then partitioned the spatial four-dimensional grid and identified the neutral helium dimer contributions as those where both electrons remain either centered within a distance of $d_{\mathrm{neutral}} = 7$ a.u. at different nuclei in the dimer or in the region between the two nuclei and within a transverse distance of $d_{\mathrm{neutral}} = 7$ a.u. Singly ionized contributions are identified by requiring that one of the two electrons remains in regions of the same shape but with $d_{\mathrm{single}} = 4$ a.u. The complementary part of the space was identified as double ionization. In test calculations we have varied the distances chosen to partition the space and found that the single and double ionization probabilities do not change significantly upon variation about the values for the distances stated above.

III. SINGLE IONIZATION

In this section we use the model Hamiltonians to study scattering effects in single photoionization of the dimer, or more precisely, the dynamical effects of the photoelectron that is emitted at one of the atoms and then scattered at the other atom in the dimer. To this end we obtained the photoelectron angular distributions by taking a Fourier transform of the contributions to the wave function that were identified as single ionization in the numerical simulations. From the results

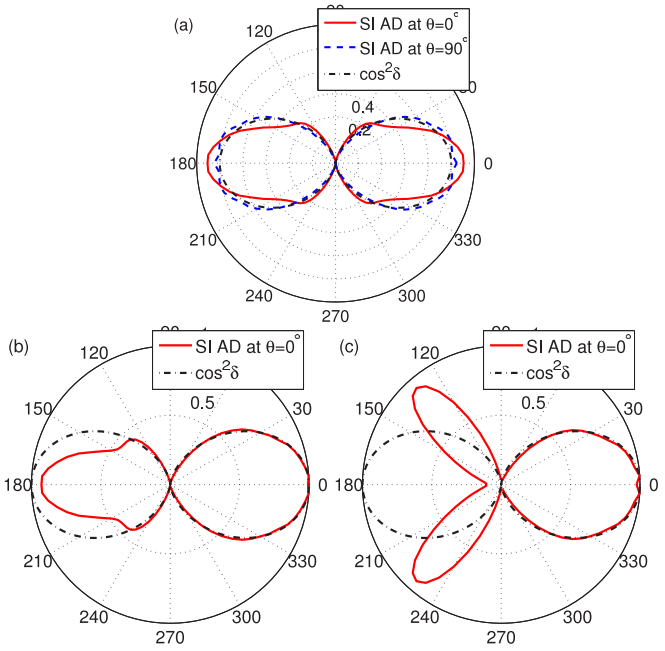

FIG. 3. (Color online) Comparison of photoelectron angular distributions in single ionization of the helium dimer using the (a) full and abridged Hamiltonians (b) $H_{\mathrm{E1,local1}}$ [Eq. (6)] and (c) $H_{\mathrm{E1,local2}}$ [Eq. (7)]. Results represented by solid lines are obtained for parallel orientation of the dimer axis with respect to the polarization direction of the field, which is chosen along the horizontal axis. For the (a) full simulations also shown is the distribution obtained for perpendicular orientation ($\theta = 90^\circ$, blue dashed line) of the dimer axis and for all simulations the distributions are compared to the expected $\cos^2$ distribution (dash-dotted lines). For the sake of comparison, the distributions in (a) are scaled such that their areas match, while in (b) and (c) the distributions are matched at one point. In all simulations a four-cycle 20 nm XUV laser pulse with a peak intensity of 1×10^{14} W/cm^2 has been used.

for the full model Hamiltonian, shown in Fig. 3(a), we see, as pointed out earlier [11], that the photoelectron angular distributions depend on the orientation of the dimer axis with respect to the polarization direction of the laser. For an orientation perpendicular to the polarization axis, the distribution (dashed line) is close to the expected p-wave distribution ($\cos^2$, dash-dotted line) for single-photon absorption from an s state. On the other hand, for parallel orientation we observe a deviation from the $\cos^2$ distribution, and the angular distribution appears to be narrower around the polarization direction with two small wings in the region between 30° and 60° with respect to the polarization axis. These deviations in the distributions were previously interpreted as an indication for the scattering of the photoelectron at the other atom in the dimer.

To shed further light on this interpretation, we present in the other panels of Fig. 3 results obtained with the abridged Hamiltonians $H_{\mathrm{E1,local1}}$ [Eq. (6), Fig. 3(b)] and $H_{\mathrm{E1,local2}}$ [Eq. (7), Fig. 3(c)] for orientation of the dimer parallel to the polarization direction. In both sets of simulations only one of the two electrons, namely electron 1, interacted with the field and, moreover, this active electron 1 was located at nucleus 1, which is the nucleus located on the right in the present figures. In this configuration we can compare photoemission with (emission to the left) and without (emission to the right) scattering at the second atom, which is located to the left of the initial position of the active electron. The result in Fig. 3(b), in which all Coulomb interactions of the active electron with the other electron and the nuclei are taken into account, confirm that the nonscattered angular distribution is close to the $\cos^2$ distribution (dash-dotted line), while the scattered angular distribution shows the deviation observed in the full simulations. This demonstrates the effect of scattering on the photoelectron angular distribution. We note that the small deviations between the numerical results and the $\cos^2$ distributions in the right part of the lobe, most notably in the kink along the polarization direction in Fig. 3(c), reflect the numerical errors in the present calculations.

We can even further distinguish between the effect of electron-electron and electron-ion scattering. This can be done by comparing the results in Figs. 3(b) and 3(c). In the latter simulations we deliberately neglected the interaction between the active electron and the second nucleus, i.e., the nucleus on the left. The comparison shows that the angular distribution for the scattered photoelectron changes. Emission of the electron along the polarization direction is now strongly suppressed, while there are two maxima at an angle of about 40° with respect to the polarization axis. Thus, we can conclude that it is the electron-electron scattering which gives rise to the two wings in the full distribution. On the other hand, the electron-nucleus (or electron-ion) scattering causes, due to the attractive nature of the interaction, a narrowing (or focusing) to the angular distribution along the polarization direction.

IV. DOUBLE IONIZATION

In this section we analyze the results of simulations using the full and abridged Hamiltonians to study the correlated electron emission from the model dimer. To this end, we first investigate the projection onto different approximate two-electron wave functions to obtain the photoelectron angular distributions. We then proceed to compare the angular distributions of the primary and the knock-off electrons.

A. Projection on the final state

The final state of double photoionization of the dimer represents a state with two electrons in the continuum of a doubly charged two-center potential. In order to obtain photoelectron angular distributions, we intend to project the respective spatial part of the wave function at the end of the simulation onto an approximate final-state wave function. Since an analytical solution of this four-body problem is not known in Cartesian coordinates, we have tested several two-electron wave functions, in which different parts of the full Coulomb interactions between the charged particles have been taken into account. To this end, we expressed the Coulomb potential between the electrons and the residual ions as well as between the two electrons in the center-of-mass [c.m., $X = (x_1 + x_2)/2$ and $Z = (z_1 + z_2)/2$] and relative coordinates ($x = x_1 - x_2$ and $z = z_1 - z_2$) of the

two electrons as

$$V(x,z;X,Z) = \frac{1}{\sqrt{x^2+z^2}} + \sum_{i,j=1}^{2} V_{\mathrm{SAE}}\left\{\left[\left(X-(-1)^i\frac{x}{2}+(-1)^j\frac{R}{2}\sin\theta\right)^2 + \left(Z-(-1)^i\frac{z}{2}+(-1)^j\frac{R}{2}\cos\theta\right)^2\right]^{1/2}\right\}. \quad (10)$$

For $|X|,|Z|,R \gg |x|,|z|$, V reduces to

$$V(x,z;X,Z) \approx V_{\mathrm{ee}}(x,z) = \frac{1}{\sqrt{x^2+z^2}}, \quad (11)$$

which suggests to approximate the final state as a product of a Coulomb wave in the relative and a plane wave in the c.m. coordinates, which we denote as ψ_{ee}. Thus, in this approximation the Coulomb interaction between the two electrons is retained while the Coulomb interactions between the electrons and the nuclei are neglected. In order to approximately test the relative importance of the Coulomb interactions in the final state, we have further considered the case in which the interaction between the electrons is neglected. As a further approximation we then assumed that the total charge of the nuclei is concentrated at the center of the coordinate system. In this approximation the full potential reduces to

$$V(x,z;X,Z) \approx V_{\mathrm{eN}}(X,Z) = -\frac{4}{\sqrt{X^2+Z^2}}, \quad (12)$$

and the final state ψ_{eN} is approximated by a product of a plane wave in the relative and a Coulomb wave in the c.m. coordinates of the electrons for a monomer with twice the residual charge. As a third option, we also considered a simple product of two plane wave functions to describe the final state wave function of the two electrons.

Since our model is planar, we used a two-dimensional scattering wave function [15,16] for the Coulomb wave,

$$\psi(\boldsymbol{k},\boldsymbol{r}) = \sum_{l=-\infty}^{\infty} \frac{e^{-\pi\eta/2}}{\sqrt{\pi}}\left|\Gamma\left(|l|+\frac{1}{2}+i\eta\right)\right| \frac{(-2i\rho)^{|l|}}{(2|l|)!} \times e^{i\rho}e^{i\sigma_{|l|}}{}_1F_1\left(|l|+\frac{1}{2}+i\eta,2|l|+1,-2i\rho\right) \times \frac{e^{il(\phi_r-\phi_k)}}{2\pi}, \quad (13)$$

where ${}_1F_1$ is the confluent hypergeometric function. Here $\boldsymbol{k}$ and $\boldsymbol{r}$ represent either the relative or c.m. momentum and displacement of two charged particles in two dimensions with k, r, ϕ_k, and ϕ_r being their magnitudes and phases, respectively. $\eta = \mu Z_1 Z_2/k$, where μ is the reduced mass of the two particles (1/2 in the case of V_{ee} and 2 in the case of V_{eN}) and Z_1 and Z_2 are their charges (-1 and -1 in the case of V_{ee} and -2 and 2 in the case of V_{eN}), $\rho = kr$, and $\sigma_{|l|} = \arg\Gamma(|l|+\frac{1}{2}+i\eta)$ is the two-dimensional Coulomb phase. Alternatively we also expressed the two-dimensional scattering wave function in terms of the three-dimensional Coulomb wave function F_l,

$$\psi(\boldsymbol{k},\boldsymbol{r}) = \sum_{l=-\infty}^{\infty}\sqrt{\frac{2}{\pi\rho}}(-i)^{|l|}e^{i\sigma_{|l|}}F_{|l|-\frac{1}{2}}(\eta,\rho)\frac{e^{il(\phi_r-\phi_k)}}{2\pi}, \quad (14)$$

which enables us to use available packages like GNU Scientific Library (GSL) for the calculation. In the practical computations we truncated the sum over l to $l_{\max} = 12$ for ψ_{ee} and $l_{\max} = 16$ for ψ_{eN}. While we found that the results for the angular momentum distributions presented below are converged for projection to ψ_{ee}, the momentum-space wave function for projection onto ψ_{eN} was not fully converged. However, we checked that our qualitative conclusions below [Figs. 4(e) and 4(f)] are correct. We attribute the difficulty in the convergence to the fact that we used a monomer Coulomb wave function for a two-center problem in ψ_{eN} and that the residual potential is not purely $1/r$. The degree of convergence can indeed be estimated by comparing the double ionization

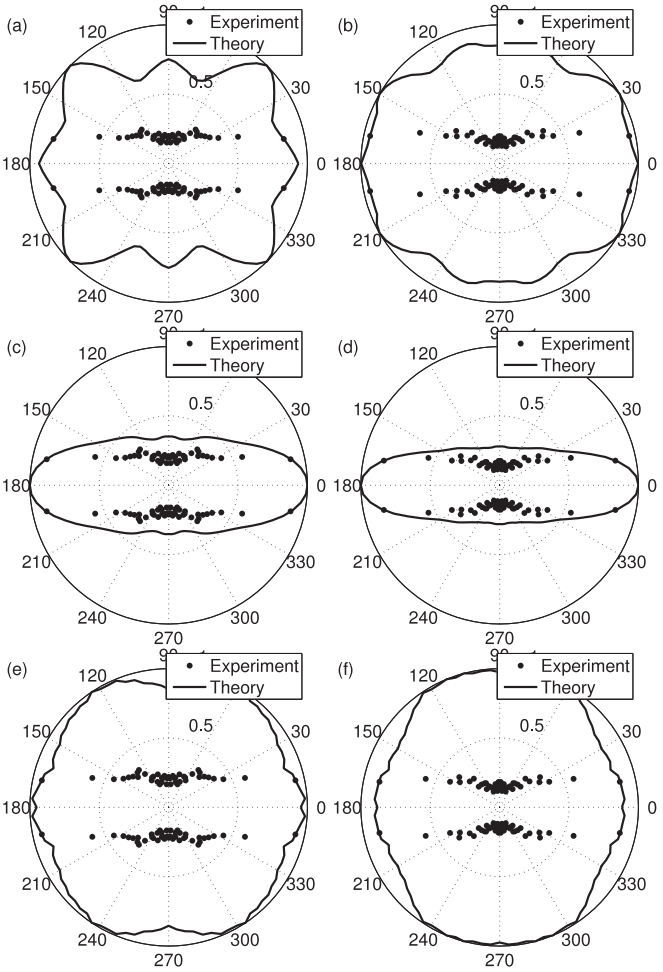

FIG. 4. Molecular-frame angular distributions of one of the two electrons in the double photoionization, obtained by projection of the respective part of the wave function onto different approximate final two-electron states at $R = 5.6$ a.u. (left column) and $R = 10$ a.u. (right column). For the results in (a) and (b), the product of two plane waves in the c.m. and relative coordinates is used as the approximate final two-electron state, while for the results in (c) and (d), ψ_{ee}, and for those in (e) and (f), ψ_{eN} is used.

TABLE I. Double ionization probabilities for the different momentum-space wave functions.

R	5.6	10
ψ_{plane}	3.5520×10^{-5}	1.9182×10^{-5}
ψ_{ee}	3.4636×10^{-5}	1.7428×10^{-5}
ψ_{eN}	1.0908×10^{-5}	6.8121×10^{-6}

probabilities obtained for the corresponding momentum-space wave function in each case, given in Table I. Evidently the probabilities of the momentum-space wave functions obtained by projection onto the product of two plane waves and onto ψ_{ee} agree rather well with each other, while the result for the projection onto ψ_{eN} indicates the lack of convergence with respect to $l_{\max}$.

In Fig. 4 we compare results for the molecular-frame angular distributions of one of the two electrons in the double photoionization after projections onto the product of two plane waves [Figs. 4(a) and 4(b)], onto ψ_{ee} [Figs. 4(c) and 4(d)], and onto ψ_{eN} [Figs. 4(e) and 4(f)]. The distributions are integrated over the emission angle of the other electron and the energies of the electrons. The theoretical data are shown in each set as a function of the emission angle of the electron. In order to compare with recently obtained experimental data [10], the theoretical results are averaged over the orientation of the dimer axis and weighted with respect to singlet and triplet state contributions according to the multiplicities of the states. Furthermore, due to the short duration of the pulse used in the simulations, the calculated distributions show a slight left-right asymmetry along the polarization direction. We have removed this asymmetry by taking the mean of the original result and its mirror image with respect to the plane perpendicular to the polarization axis through the center of mass of the two nuclei. Finally, the theoretical results are matched to coincide with the experimental data at the maximum of the distributions. The comparison shows that within the present model the approximation of the final-state wave function as product of a plane wave in the c.m. coordinates and a Coulomb wave in the relative coordinates qualitatively appears to be the most appropriate in one of the three considered options. We therefore used ψ_{ee} to obtain angular distributions for the remainder of our studies.

B. Angular distributions of primary and knock-off electrons

In previous studies it has been found [10,11] that the double photoionization of the helium dimer proceeds via the so-called knock-off mechanism for low photon energies. According to this mechanism, first the primary electron gets ionized after interaction with the field and then shares its energy via collisional impact ionization with the second knock-off electron. As mentioned above we can distinguish between the two electrons by restricting the electron-field interaction to one of the two electrons and locating the electrons at one of the atoms in the dimer.

In Fig. 5 we present results of simulations with the different abridged model Hamiltonians [Eqs. (6) and (7)]. In the panels in the left column the angular distributions of the primary electron, i.e., the electron interacting with the field, are presented, while in the right column those of the knock-off electron are shown. In all cases the dimer was oriented along the polarization axis, which is the horizontal axis in each of the panels. We have integrated the distributions over the emission angle of the other electron and the energies of the two electrons.

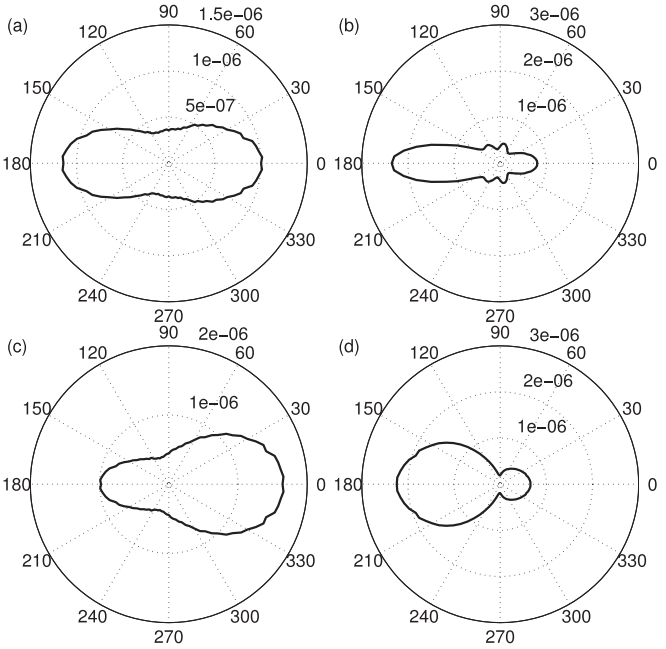

FIG. 5. Angular distribution of the primary (left column) and knock-off electron (right column) in double photoionization of the helium dimer. Results from simulation with different abridged Hamiltonians are compared: (a) and (b) correspond to $H_{\text{E1,local1}}$ [Eq. (6)] and (c) and (d) correspond to $H_{\text{E1,local2}}$ [Eq. (7)]. In each of the simulations a four-cycle 20 nm XUV laser pulse with a peak intensity of 1×10^{14} W/cm^2 and parallel orientation of the dimer axis with respect to the polarization direction of the field (along the horizontal axis of the figure) was considered.

Due to the location of the electrons in our models we can study the emission direction of the electrons with respect to their initial location in the dimer as well as the role of electron-nucleus and electron-electron interaction during the impact ionization. The result in Fig. 5(a), obtained using $H_{\text{E1,local1}}$ [Eq. (6)], in which all interactions of the primary electron are retained, shows that the primary electron is scattered both in forward and backward directions with respect to the propagation direction (from right to left in the figure) after absorption of the photon. Further restriction by suppression of the electron-nucleus scattering in the energy transfer process $H_{\text{E1,local2}}$ [Eq. (7)] reveals that the electron-electron scattering favors backward scattering of the primary electron, as expected in a head-on collision from a repulsive center [Fig. 5(c)].

On the other hand, the knock-off electron is predominantly ionized along the momentum direction of the incoming primary electron in the impact ionization process, cf. Figs. 5(b) and 5(d). The contribution from the electron-electron interaction leads to a rather broad angular distribution with respect to the molecular axis [Fig. 5(d)], in agreement with

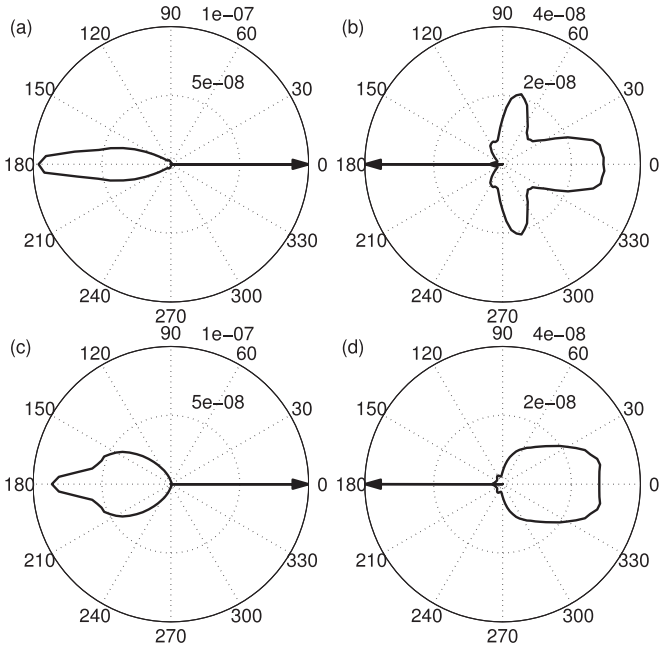

FIG. 6. Angular distributions of the knock-off electron in double photoionization obtained using (a) and (b) $H_{\mathrm{E1,local1}}$ [Eq. (6)] and (c) and (d) $H_{\mathrm{E1,local2}}$ [Eq. (7)]. The emission of the primary electron was fixed along the direction indicated by the arrow. The field parameters were the same as in Fig. 5.

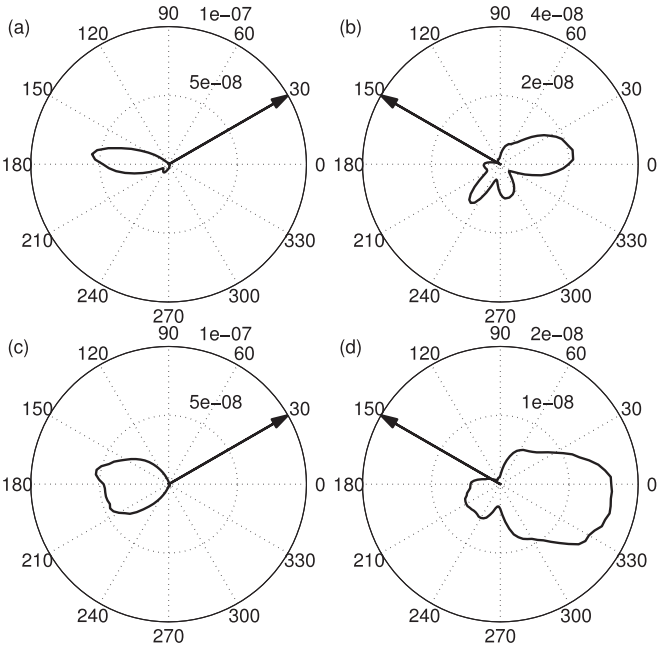

FIG. 7. Same as Fig. 6, but for different emission direction of the primary electron.

a similar distribution of the primary electron in the opposite direction [Fig. 5(c)]. The inclusion of the electron-nuclear contribution leads to a distribution which is more aligned along the polarization direction [Fig. 5(b)].

Finally, we obtained the angular distributions of the knock-off electron when the primary electron is fixed along certain emission directions. For the results presented in Fig. 6 we considered emission of the primary electron either in backward (with respect to the impact direction, panels on the left) or forward direction (panels on the right), using abridged Hamiltonians $H_{\mathrm{E1,local1}}$ [Eq. (6), Figs. 6(a) and 6(b)] and $H_{\mathrm{E1,local2}}$ [Eq. (7), Figs. 6(c) and 6(d)]. The distributions show that the two electrons are predominantly emitted back-to-back in particular for backward scattering of the primary electron. As can be seen in the distributions, we observe for backward scattering that inclusion of electron-nucleus interaction leads to a stronger alignment of the distribution along the direction of electron impact [cf. Figs. 6(a) and 6(c)]. On the other hand, for forward direction we see pronounced wings in the angular distributions of the knock-off electron when $H_{\mathrm{E1,local1}}$ is used where all interactions of the primary electrons are included [Fig. 6(b)].

Similar conclusions hold for other emission angles of the primary electron with respect to the molecular axis and the polarization direction as well, as can be seen from the results presented in Fig. 7. In general, we observe that the electrons are predominantly emitted in opposite half planes to the polarization direction. For backward scattering of the primary electron, inclusion of the electron-nucleus interaction leads to a narrower angular distribution of the knock-off electron.

V. SUMMARY

We have shown how scattering effects in single and double photoionization of the helium dimer can be studied in *ab initio* numerical simulations. Due to the large internuclear separation in the dimer, the interaction between the electrons and between each electron and the distant nucleus in the ground state of the dimer is small. This has enabled us to consider abridged Hamiltonians for the dimer model, in which these interactions are neglected without changing the initial state significantly. Based on the comparison of angular distributions of the primary photoelectron and the secondary knock-off electron obtained with different abridged Hamiltonians in numerical simulations, we were able to identify the role of the different Coulomb interactions. For single photoionization our results show that the electron correlation interaction leads to scattering of the photoelectron off the dimer axis, when the latter is oriented along the polarization direction of the field. On the other hand, the electron-nucleus interaction tends to focus the electron along the polarization direction. In double photoionization the primary photoelectron is scattered both in forward as well as backward direction with respect to its initial momentum direction obtained upon photon absorption. Keeping the direction of the primary electron fixed we then further found that the two electrons are primarily emitted back-to-back in the double photoionization process.

ACKNOWLEDGMENTS

We thank J. Su, C. Ruiz, and R. Dörner for stimulating discussions. Support via grants from the U.S. National Science Foundation (Grants No. PHY-0854918 and No. PHY-1125844) is acknowledged. This work utilized the Janus supercomputer, which is supported by the National Science

Foundation (Grant No. CNS-0821794) and the University of Colorado Boulder. The Janus supercomputer is a joint effort of the University of Colorado Boulder, the University of Colorado Denver, and the National Center for Atmospheric Research. Janus is operated by the University of Colorado Boulder.

[1] T. N. Rescigno, M. E. Baertschy, W. A. Isaacs, and C. W. McCurdy, Science **286**, 2474 (1999).
[2] H. Bachau, E. Cormier, P. Decleva, J. E. Hansen, and F. Martin, Rep. Prog. Phys. **64**, 1815 (2001).
[3] R. Dörner, V. Mergel, O. Jagutzki, L. Spielberger, J. Ullrich, R. Moshammer, and H. Schmidt-Böcking, Phys. Rep. **330**, 95 (2000).
[4] J. S. Briggs and V. Schmidt, J. Phys. B **33**, R1 (2000).
[5] F. Krausz and M. Ivanov, Rev. Mod. Phys. **81**, 163 (2009).
[6] T. Popmintchev, M. C. Chen, P. Arpin, M. Murnane, and H. Kapteyn, Nat. Photon. **4**, 822 (2010).
[7] W. Ackermann *et al*., Nat. Photon. **1**, 336 (2007).
[8] T. Shintake *et al*., Nat. Photon. **2**, 555 (2008).
[9] P. Emma *et al*., Nat. Photon. **4**, 641 (2010).
[10] T. Havermeier, T. Jahnke, K. Kreidi, R. Wallauer, S. Voss, M. Schöffler, S. Schössler, L. Foucar, N. Neumann, J. Titze, H. Sann, M. Kühnel, J. Voigtsberger, A. Malakzadeh, N. Sisourat, W. Schöllkopf, H. Schmidt-Böcking, R. E. Grisenti, and R. Dörner, Phys. Rev. Lett. **104**, 153401 (2010).
[11] H. Ni, C. Ruiz, R. Dörner, and A. Becker, Phys. Rev. A **88**, 013407 (2013).
[12] J. A. R. Samson, Phys. Rev. Lett. **65**, 2861 (1990).
[13] X. M. Tong and C. D. Lin, J. Phys. B **38**, 2593 (2005).
[14] R. A. Aziz and M. J. Slaman, J. Chem. Phys. **94**, 8047 (1991).
[15] L. S. Davtyan, G. S. Pogosyan, A. N. Sisakyan, and V. M. Ter-Antonyan, Theor. Math. Phys. **74**, 157 (1988).
[16] X. L. Yang, S. H. Guo, F. T. Chan, K. W. Wong, and W. Y. Ching, Phys. Rev. A **43**, 1186 (1991).